DE GRUYTER Open Geosciences 2020; 12: 887–903

Research Article

Chun-Hui Xu, Lin-Fu Xue*, and Chong Peng

Constraints of nonseismic geophysical data on the deep geological structure of the Benxi iron-ore district, Liaoning, China

https://doi.org/10.1515/geo-2020-0190
received May 10, 2019; accepted August 28, 2020

Abstract: The Benxi area in Liaoning Province is one of the most important iron-ore districts in China. This study uses nonseismic geophysical data (in the form of gravity–magnetic–magnetotelluric data) and based on the section modeling method to model the deep, three-dimensional geological structure of the Benxi area. Based on the modeling results and deep geological structure characteristics, the Benxi area can be divided into three first-order deep geological tectonic units. A close relationship is between tectonic unit and iron-ore concentrations. First, high-quality iron-ore deposits occur within the tectonic boundary and sedimentary boundary zone of the Jiao–Liao–Ji Belt, reflects the protective effect of sedimentary cover on the iron-bearing formation. Second, enriched iron-ore deposits are mainly developed in Mesozoic granitic intrusion zone, reflects the hydrothermal leaching of silicon in host iron-bearing formations during magma intrusion. Thus, the findings of this study have important implications for future prospecting in the Benxi iron-ore district.

Keywords: deep geological structure, nonseismic geophysical profile, BIF iron ore, Mesozoic intrusive rock, three-dimensional geological model

1 Introduction

The Anshan-Benxi (An-Ben) area (Figure 1b) in Liaoning, China, hosts an important Neoarchean banded iron formation (BIF) deposit, accounting for 40% of China's BIF-derived iron-ore resources [1]. Extensive research has already been conducted on the genesis, age, and environment of formation of the An-Ben deposit and the enrichment of the hosted iron ore. Existing studies suggest that the An-Ben BIF is of the Algoma type, and formed in Neoarchean (~2.55–2.50 Ga) [2–5], formed by chemical deposition of silicon and iron materials brought by submarine volcanic hydrothermal jet [6–10]. The An-Ben BIF was subjected to intense metamorphism and deformation during the later stages of its deposition since it deposited [11,12].

Since the beginning of the 21st century, deep iron-ore mining has expanded in the An-Ben area, and the focus of iron ore research turned to supplementary mine surveys and general exploration. In 2006, the Dataigou super-large iron-ore deposit was discovered at a depth of ~1,100–1,200 m beneath the Paleoproterozoic sedimentary cover in DaTaigou, Benxi, and the resources of this deposit have been estimated about ~3.4 billion tons [13]. The discovery of the Dataigou deposit suggests the potential for deep iron-ore deposits in the An-Ben area, and which generates significant interest in the deep geological structure of the area. Fan et al. [14] integrated gravity and magnetic inversion data to establish a geological profile between Donganshan and Qidashan to a depth of 5 km to predict the occurrence of large iron-ore bodies beneath the Anshan area. Peng et al. [15] used nonseismic geophysical data to determine the subsurface geological structure of the An-Ben area and identified the basin-controlling boundary fault of the Jiao–Liao–Ji Belt. In addition, Xue et al. [12] established a three-dimensional (3-D) inversion map of the magnetic susceptibility of the Anshan area via integrated analysis of aeromagnetic, magnetic susceptibility, and structural

---

*** Corresponding author: Lin-Fu Xue,** College of Earth Sciences, Jilin University, Changchun 130061, China, e-mail: jldxxlf@sina.com
Chun-Hui Xu: College of Earth Sciences, Jilin University, Changchun 130061, China; College of Tourism and Geographical Sciences, Jilin Normal University, Siping 136000, China, e-mail: 252143580@qq.com
Chong Peng: College of Earth Sciences, Jilin University, Changchun 130061, China; College of Geographical Sciences, Shanxi Normal University, Linfen 041004, China, e-mail: 137505175@qq.com

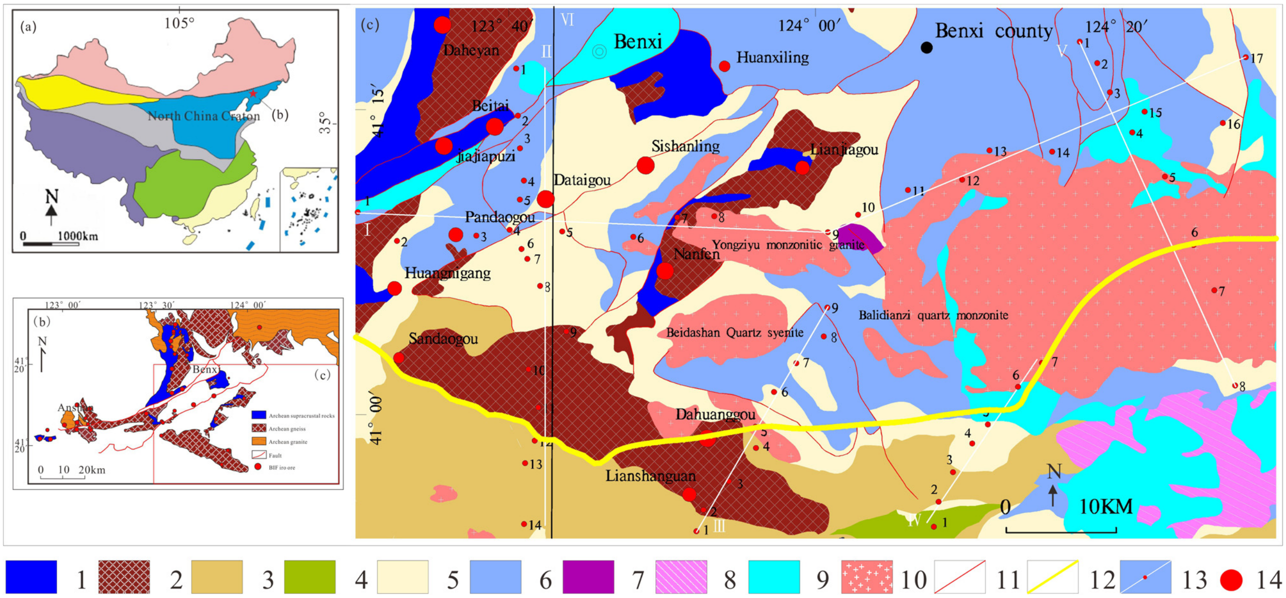

Figure 1: (a) The location of the North China Craton in China; (b) The distribution diagram of BIF iron deposit in Anshan-Benxi area; (c) Simplified geological map of Benxi area. (2) Archean gneiss. (3) Paleoproterozoic unit. (4) Paleoproterozoic granite. (5) Neoproterozoic unit. (6) Paleozoic unit. (7) Early Triassic basic-ultrabasic complexes. (8) Late Triassic alkaline complex. (9) Mesozoic unit. (10) Mesozoic granite. (11) Fault. (12) Tectonic boundary of Jiao-Liao-Ji Belt (Peng et al., 2016). (13) Locations of MT measurement lines and points. (14) BIF iron ore.

data; those authors estimated that iron-ore deposits in the Anshan area could extend down to depths of 5,600 m, implying significant prospecting potential.

But knowledge of the deep geological structures in An-Ben area (Figure 1c) remains fuzzy. In this paper, to better constrain the deep geological structures of the Benxi area, high-precision gravity–magnetic–magnetotelluric (MT) surveys were conducted.

2 Regional geological background

Neoarchean BIF deposits in Benxi, China, are located in the transition zone between the northern boundary of the Jiao–Liao–Ji Belt and the Longgang Block, which is situated in the eastern segment of the northern margin of the North China Craton (Figure 1c; [15]). The Jiao–Liao–Ji Belt is characterized by Paleoproterozoic meta-sedimentary rock sequences that are dominated by phyllite, granulite, schist, and marble [16]. In some areas, Paleoproterozoic intrusions, consisting of streaked monzonitic granites, granodiorites, and granites, also occur [17,18]. The Longgang Block has a double-layered structure comprising crystalline basement overlain by sedimentary cover. The crystalline basement is composed mainly of Archean supracrustal rocks and Neoarchean granitic gneiss. The Archean supracrustal rocks belong to the iron-bearing formation, which is called the Anshan Group in the An-Ben area, with the main lithologies of amphibolite, biotite granulite, magnetite quartzite, silica–dolomite quartz schist, and chlorite schist. The Neoarchean granitic gneiss consists mainly of monzonitic granitic gneiss, quartz diorite gneiss, and granitic gneiss. The sedimentary cover formed in Neoproterozoic–Paleozoic; the Neoproterozoic rocks comprise predominantly mudstone, shale, and quartz sandstone, whereas the Paleozoic rocks are mainly carbonates and terrigenous clastics.

The Benxi area underwent a phase of intense magmatic activity and fault-related subsidence during the Mesozoic. The Late Jurassic Yongziyu monzonitic granite, intruding Neoarchean–Paleozoic rocks, crops out as an elongate, E–W-oriented stock over an area of ~65 km^2. The Early Cretaceous Balidianzi quartz monzonite has an acurate distribution and crops out over an area of ~16 km^2. This quartz monzonite intruded the Neoproterozoic, Paleozoic, and Mesozoic strata as well as Late Triassic Xuetun basic-ultrabasic rocks and an Early Cretaceous rhyolite porphyry. The Early Cretaceous Beidashan quartz syenite has an oval-shaped distribution with an area of ~34 km^2, and intruded the Neoproterozoic and Paleozoic rocks and the Balidianzi quartz monzonite.

The Dataigou deposit contains iron-ore reserves of >3 billion tons, the Sishanling deposit with reserves of

2.48 billion tons, and the Nanfen deposit, which hosts reserves of 1.29 billion tons. Additional deposits containing reserves of >100 million tons are found at Beitai, Jiajiapuzi, Daheyan, and seven smaller sites, including Huanxiling and Lianjiagou [13,19,20].

There are two dominant sets of faults in the study area, trending NE–SW and NW–SE, respectively. The NE–SW-trending faults are mainly Hanling–Pianling fault zone and its branch faults, the Hanling–Pianling Fault zone has great significance to the Stratigraphy before the cenozoic, magmatic activity, volcanic eruptions and the exploration of BIF deposits in the study area. The dynamic mechanism of the formation is mainly related to the interaction and movement direction change of the Eurasian Sino Korean plate, Yangtze plate, izonaqi plate, Pacific plate, etc. in the Mesozoic [21]. In contrast, the NW–SE trending faults typically occur within geological bodies.

3 Rock physical characteristics

To determine the physical properties of the main lithologies in the study area, more than 1,000 samples were collected for measurements of density, magnetic susceptibility, and resistivity. The samples are representative rocks or ores of various strata or intrusive rocks collected in the field, and each rock type included at least 15 samples. Tables 1 and 2 show the types of rocks and the results of physical property analysis. The Archean strata are characterized by high densities of 3.00–3.93 g/cm^3 and high magnetic susceptibilities of 3,000–1,00,000 ($4\pi \times 10^{-6}$ SI). The Paleoproterozoic metamorphic strata also have high densities, ranging from 2.6 to 2.74 g/cm^3, but only moderate magnetic properties, with magnetic susceptibilities ranging from 50 to 2,872 ($4\pi \times 10^{-6}$ SI); they are also characterized by low resistivities. The Neoproterozoic sedimentary strata have lower densities of between 2.56 and 2.7 g/cm^3, low magnetic susceptibilities between 63 and 366 ($4\pi \times 10^{-6}$ SI), and medium resistivities. The lower Paleozoic strata possess high densities of 2.6–2.72 g/cm^3, low magnetic susceptibilities of 74–159 ($4\pi \times 10^{-6}$ SI), and low resistivities. The upper Paleozoic strata also have low magnetic susceptibilities and low resistivities, and slightly lower densities ranging from 2.6 to 2.63 g/cm^3. The Mesozoic strata are characterized by low densities, low magnetic susceptibilities, and low resistivities.

The acidic intrusive rocks in the study area are typified by high resistivities of 26,216–2,12,910 Ωm and low densities between 2.53 and 2.64 g/cm^3 but possess varying magnetic susceptibilities. The Mesozoic intrusive rocks have the highest magnetic susceptibility, ranging from 153 to 2,512 ($4\pi \times 10^{-6}$ SI), followed by the Archean and then the Paleoproterozoic intrusive rocks, which have magnetic susceptibilities ranging from 13 to 194 ($4\pi \times 10^{-6}$ SI). The density of the Archean intrusive rocks is slightly higher than those of the Mesozoic intrusive rocks and the Paleoproterozoic intrusive rocks.

Table 1: Statistical tables of major strata physical properties in the study area

Ages	Lithology	Number of specimens	Resistivity (Ωm)	Magnetic susceptibility ($4\pi \times 10^{-6}$ SI)	Density (g/cm^3)
Mesozoic	Tuff	30	1,512	727	2.63
	Sandy slate	25	8,536	−15.76	2.51
	Pyroclastic rock	20	18,844	116	2.62
	Sandstone	20	20,714	11.41	2.63
Upper Paleozoic	Sandstone	80	691	148	2.63
Lower Paleozoic	Limestone	120	4,413	195	2.71
	Muddy limestone	40	2,456	108	2.70
	Muddy limestone	35	4,643	157	2.72
	Crystallized limestone	15	2,186	360	2.73
	Quartz sandstone	100	392	143	2.71
Neoproterozoic	Quartz sandstone	160	3,565	148	2.64
	Muddy limestone	45	1,223	160	2.7
	Silicified quartz sandstone	50	948	126	2.6
Paleoproterozoic	Banded marble	25	2,977	159	2.74
	Biotite plagioclase schist	95	1,483	137	2.7
	Marble	55	1,330	613	2.76
Archean	Magnetite-quartzite	20	344	1,47,984	3.18

Table 2: Statistical tables of major intrusive rocks physical properties in the study area

Ages	Lithology	Number of specimens	Resistivity (Ωm)	Magnetic susceptibility ($4\pi \times 10^{-6}$ SI)	Density (g/cm^3)
Mesozoic	Granite	20	1,13,785	268	2.53
	Adamellite	34	1,65,096	712	2.53
	Quartz monzonite	25	2,11,910	153	2.6
	Monzonitic granite	25	2,11,909	2,512	2.61
	Muscovite syenite	40	319	1,184	2.54
Paleoproterozoic	Granite Granodiorite	130	1,69,915	194	2.62
	Biotite plagiogranite	20	1,27,644	13	2.59
Archean	Granitic gneiss	15	1,76,021	345	2.63

4 Acquisition and processing of nonseismic geophysical data

Five high-precision gravity–magnetic–MT data in Benxi area were conducted by Jilin University (Figure 1c). Gravity measurements were made using a Burris-type, high-precision gravimeter with a standard screw accuracy of ±0.01 mGal and a dot pitch of 250 m. The measured regional Bouguer anomalies were a mixture of zero-point corrections, latitude corrections, terrain corrections, and Bouguer corrections of gravity differences, with a mean squared error of 0.245×10^{-5} m/s^2. The terrain corrections of the gravity data were divided into near-area (0–50 m), medium-area (50–2,000 m), and two far-area corrections (I: $2 \times 103^{-20} \times 10^3$ m, II: 20×10^3–166.7×10^3 m), with a maximum radius for terrain corrections of 166.7×10^3 m and a mean layer density of 2.67×10^{-3} kg/m^3 used to calculate the terrain corrections.

A GSM-19T Microcomputer Proton Magnetometer (GEM, Canada) with sensitivities of ~0.01 nT was used to obtain magnetic data. In order to ensure the consistency of data, the magnetic measurement points and the gravity measurement points were in the same position. Magnetic data processing corrections included daily variations, normal field, and altitude, yield a minimum correction value of 0.1 nT and a mean squared error of 2.48 nT. The Benxi County is the base point of the high-precision magnetic survey, where the normal field is 53574.36 nT.

MT measurements were made using a V5-2000 (Phoenix, Canada) with a dot pitch of 3–5 km. The measurements were taken over a period of more than 12 h. According to the quality classification standard, the excellent rate of the obtained apparent resistivity curve is more than 95%. The TM mode was used to process MT data, to improve the accuracy of the TM curve, the impedance tensor was rotated to the orientation of the vertical measuring line prior to inversion to ensure that all the measured data rotate in the same direction. Because of the high variability in the resistivities of the different sub-surface lithologies, logarithmic resistivity values were used during inversion. The MT data inversion was performed using SCS2D smoothing inversion software. For 2D inversion, the thickness of the first layer was set to 50 m, the ratio coefficient was 1.21, and the inversion depth was ~10 km.

5 Deep geological structures inferred from the nonseismic geophysical profiles (NGPs)

Integrate each processed gravity–magnetic–MT data into the same coordinate starting point obtained five NGPs (Figures 2–6), these NGPs are crucial for revealing the deep geological structure of Benxi area.

5.1 The deep geological structure, NGP I

NGP I (Figure 2), a geological body ($Ar_{3\text{-}1}$) with high resistivity (10^6 Ω m) and moderate gravity and magnetic anomalies, is observed. Archean gneiss is exposed in the same location, and so $Ar_{3\text{-}1}$ is inferred to be Archean gneiss. The high magnetic anomaly (1,800 nT) observed at survey points 4–5 is located in the area of the Dataigou iron-ore deposit, and thus the anomaly is attributed to the presence of iron ore. Survey points 4–6 are located in the Taizi River Depression, where there is a syncline structure; the strata in this location comprise a younging-upwards sequence of Archean supracrustal rocks and Paleoproterozoic and Neoproterozoic sediments. The thickness of the sedimentary cover is greater

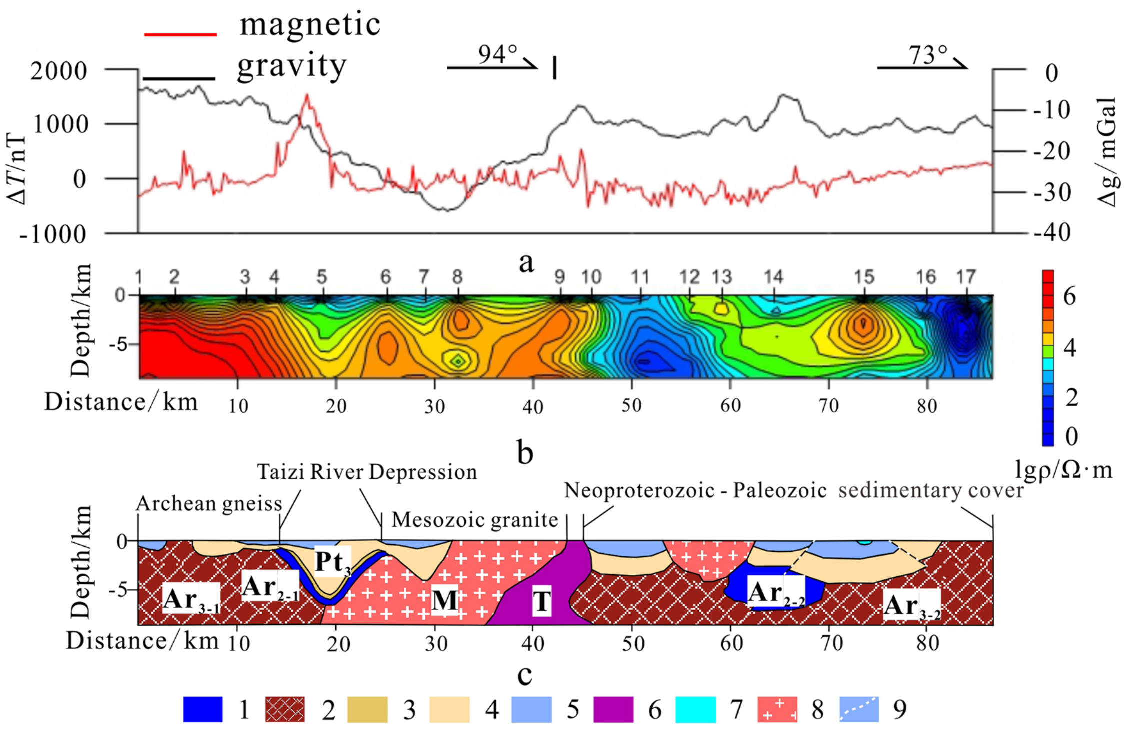

Figure 2: Nonseismic geophysical profile I. (a) Measured profile of gravity data and geomagnetic data. (b) 2D inversion profile of telluric electromagnetic soundings. (c) Inferred tectonic profiles. (1) Archean supracrustal rocks. (2) Archean gneiss. (3) Paleoproterozoic unit. (4) Neoproterozoic unit. (5) Paleozoic unit. (6) Early Triassic basic – ultrabasic complex. (7) Mesozoic unit. (8) Mesozoic granite. (9) Auxiliary line.

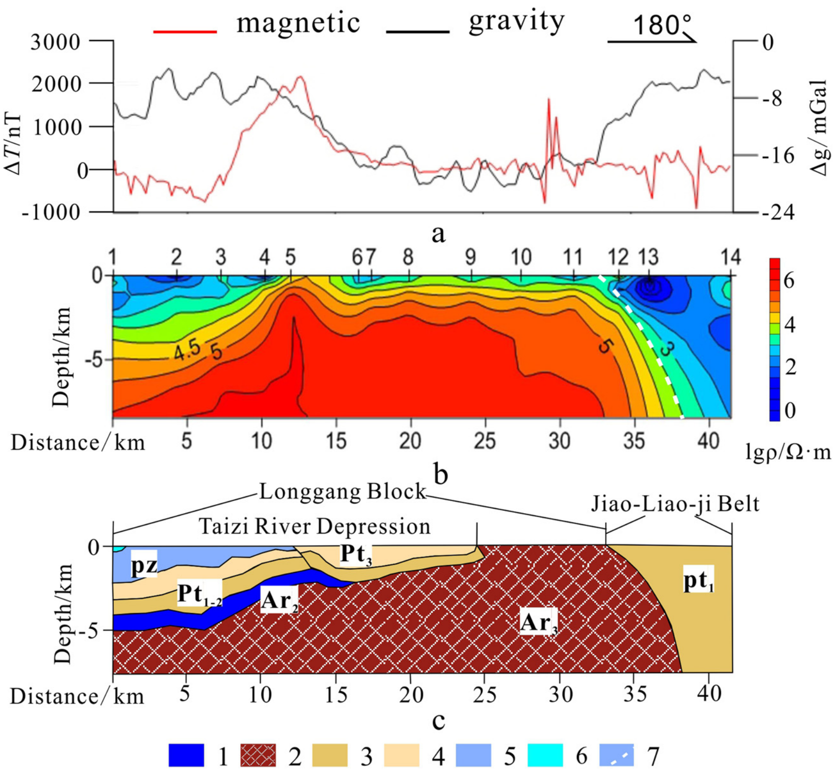

Figure 3: Nonseismic geophysical profile II. (a) Measured profile of gravity data and geomagnetic data. (b) 2D inversion profile of telluric electromagnetic soundings. (c) Inferred tectonic profiles. (1) Archean supracrustal rocks. (2) Archean gneiss. (3) Paleoproterozoic unit. (4) Neoproterozoic unit. (5) Paleozoic unit. (6) Mesozoic unit. (7) Auxiliary line.

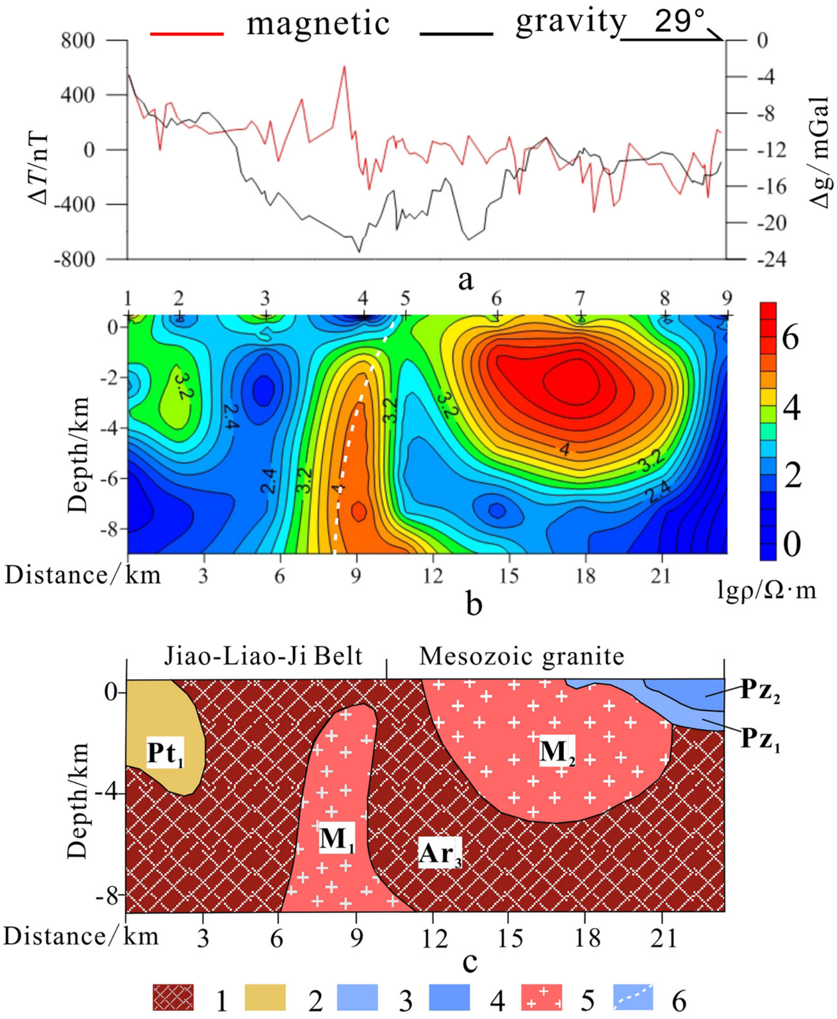

Figure 4: Nonseismic geophysical profile III. (a) Measured profile of gravity data and geomagnetic data. (b) 2D inversion profile of telluric electromagnetic soundings. (c) Inferred tectonic profiles. (1) Archean gneiss. (2) Paleoproterozoic unit. (3) Lower Paleozoic unit. (4) Upper Paleozoic unit. (5) Mesozoic granite. (6) Auxiliary line.

than 5 km at survey point 5. The identified geological body M is characterized by a high resistivity ($10^5\,\Omega$ m), a high magnetic anomaly (700 nT), and a low gravity anomaly (−35 mGal). Corresponding rock exposures consist of Mesozoic granite, and thus it is assumed that M is Mesozoic granite. Geological body $Ar_{3\text{-}2}$ is associated with a low magnetic anomaly and a high gravity anomaly and is inferred to be Archean gneiss also. This body is also characterized by low resistivity, possibly due to increased permeability, as suggested by the presence of fractures at survey points 10–11 and 17. Geological body $Ar_{2\text{-}2}$ is characterized by high gravity (−5 mGal) and magnetic (500 nT) anomalies. This body is inferred to be composed of Archean supracrustal rocks, and thus it may be a potential iron-ore reserve.

According to the deep geological structure characteristics of NGP I, the crustal structure along NGP I can be divided into four structural units: (1) between survey points 1 and 4, Archean basement rocks are either shallow or exposed; (2) between survey points 4 and 6, there is a thicker sedimentary cover; (3) survey points 6–10 are located in the area of a Mesozoic granite intrusion, where Mesozoic granites are exposed at the surface, and large rock masses occur underground; and (4) between survey points 10 and 17, there is a two-layer upper-crustal structure, comprising Neoproterozoic–Paleozoic sedimentary cover overlying Archean basement gneiss.

5.2 The deep geological structure, NGP II

NGP II (Figure 3), a low magnetic anomaly and high gravity anomaly are observed between survey points 1

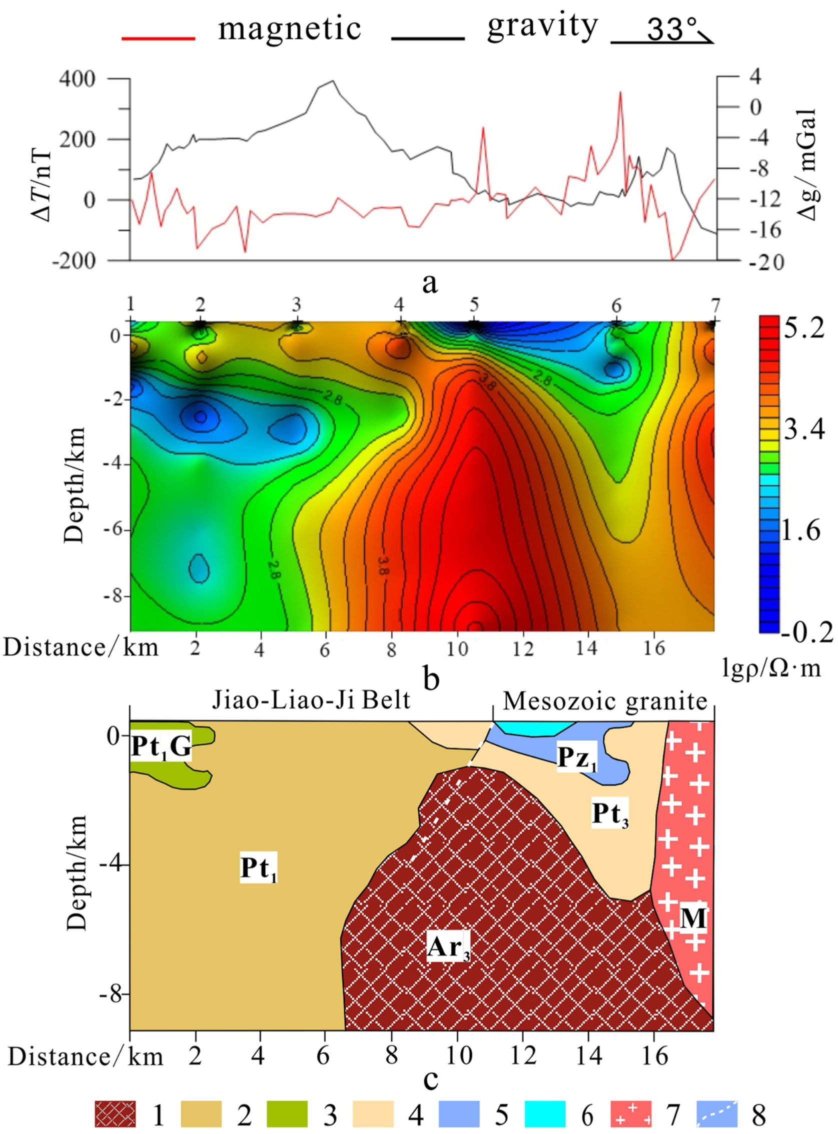

Figure 5: Nonseismic geophysical profile IV. (a) Measured profile of gravity data and geomagnetic data. (b) 2D inversion profile of telluric electromagnetic soundings. (c) Inferred tectonic profiles. (1) Archean gneiss. (2) Paleoproterozoic unit. (3) Paleoproterozoic granite. (4) Neoproterozoic unit. (5) Paleozoic unit. (6) Mesozoic unit. (7) Mesozoic granite. (8) Auxiliary line.

and 9, and the resistivity data suggest that the rocks in these locations are layered.

Geological body Pz_1 has a high gravity anomaly, a low magnetic anomaly, and low resistivity (10 Ωm), lower Paleozoic strata are exposed, it is inferred that geological body Pz_1 comprises lower Paleozoic strata. Geological body Pt_3 has a low gravity anomaly, a low magnetic anomaly, and low resistivity (10^2 Ωm), geological body Pt_3 is inferred to be Neoproterozoic strata. Geological body $Pt_{1\text{-}2}$ has a low gravity anomaly, a low magnetic anomaly and low resistivity ($10^{2.5}$ Ωm), geological body $Pt_{1\text{-}2}$ is inferred to be Paleoproterozoic Longzishan Formation. Geological body Ar_2 has a high gravity anomaly, a high magnetic anomaly, and low resistivity (10^3 Ωm), it is inferred that Ar_2 is Archean supracrustal rocks.This area is located in Taizi River Depression, with syncline structure, and the thickest sedimentary cover is 5 km. The high magnetic anomaly (2,000 nT) at survey points 4–5 likely reflects the presence of the Dataigou iron ore.

Near survey point 12, there is a sharp increase in the gravity anomaly and a sharp decrease in both the magnetic anomaly and the resistivity from north to south, it is speculated that it has a normal fault zone, with tends to the SW, the inclination is 50°. Geological body Ar_3 in the northern part of the fault zone exhibits

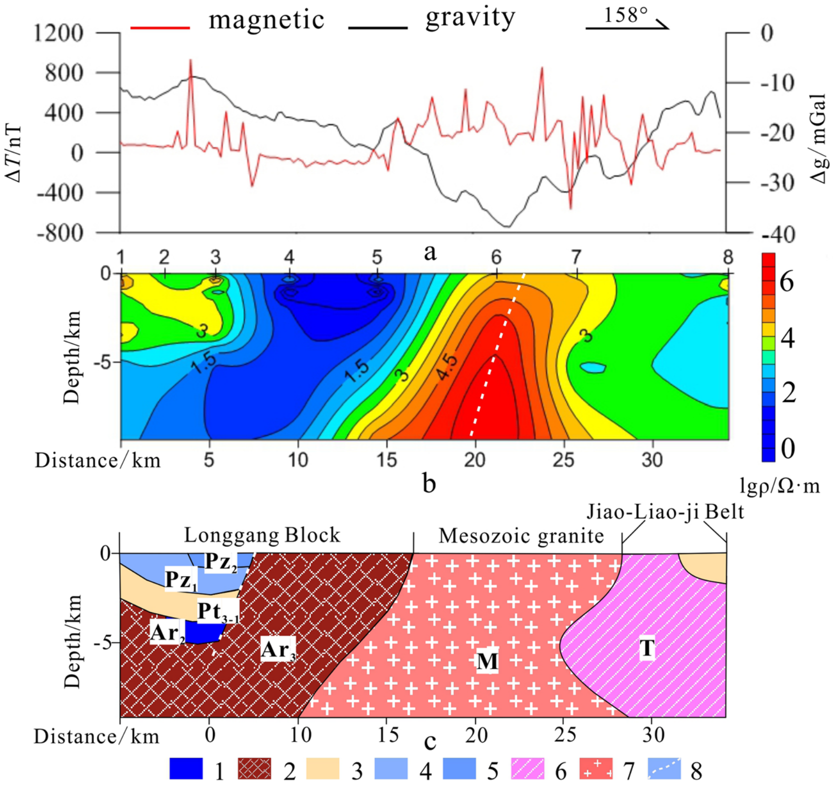

Figure 6: Nonseismic geophysical profile V. (a) Measured profile of gravity data and geomagnetic data. (b) 2D inversion profile of telluric electromagnetic soundings. (c) Inferred tectonic profiles. (1) Archean supracrustal rocks. (2) Archean gneiss. (3) Neoproterozoic unit. (4) Lower Paleozoic unit. (5) Upper Paleozoic unit. (6) Late Triassic alkaline complex. (7) Mesozoic granite. (8) Auxiliary line.

high resistivity (10^6 Ωm) and high magnetic susceptibility. Ar_3 is located in an area where Archean gneiss is exposed at the surface, and thus this body is inferred to be Archean gneiss. Geological body Pt_1 in the southern part of the fault zone exhibits low resistivity (10 Ωm) along with a moderate magnetic anomaly and a high gravity anomaly (−4 mGal). Pt_1 is located in an area where Paleoproterozoic strata are exposed, and thus, this body is inferred to be Paleoproterozoic strata. The fault is inferred to be a basin-controlling fault of the Jiao–Liao–Ji Belt. The structural unit to the south of the fault is the Jiao–Liao–Ji Belt, and the structural unit to the north of the fault is the Longgang Block.

5.3 The deep geological structure, NGP III

NGP III (Figure 4), geological body Pt_1 is characterized by moderate resistivity, a moderate magnetic anomaly, and a high gravity anomaly (−4 mGal). Corresponding outcrops consist of rocks of the Paleoproterozoic Liaohe Group, suggesting that Pt_1 may also comprise Paleoproterozoic strata. Geological body M_1 exhibits high resistivity ($10^{5.5}$ Ωm), a high magnetic anomaly (700 nT), and a low gravity anomaly (−24 mGal), characteristic of Mesozoic granite. Geological body M_2 exhibits high resistivity (10^6 Ωm) and a low gravity anomaly (−20 mGal), in a location where Mesozoic granite is exposed; thus, it is presumed that M_2 comprises Mesozoic rocks. Geological body Ar_3 is characterized by low resistivity and moderate gravity and magnetic anomalies, and the corresponding rock exposures consist of Archean gneiss. It is inferred that Ar_3 is also Archean gneiss and that its resistivity is relatively low owing to the presence of fluid-filled fractures.

The crustal structure along NGP III can be divided into two structural units: the Jiao–Liao–Ji Belt in the south and a Mesozoic granite intrusion zone in the north.

5.4 The deep geological structure, NGP IV

NGP IV (Figure 5), geological body Pt_1G is characterized by moderate resistivity, a moderate magnetic anomaly, and a low gravity anomaly (−12 mGal), in a location where Paleoproterozoic granite is exposed, and thus it is inferred that geological body Pt1G is Paleoproterozoic granite. Geological body Pt_1 exhibits a high gravity anomaly (4 mGal), a moderate magnetic anomaly, and low resistivity. The outcrops corresponding to the location of Pt_1 are of the Paleoproterozoic Liaohe Group, and thus Pt_1 is inferred to comprise Liaohe Group strata. At survey points 4–6, the gravity anomaly is low, and the magnetic susceptibility is high. The resistivity gradually increases with depth, suggesting the presence of layered strata. A syncline structure is inferred, which comprises a younging-upwards sequence of Neoproterozoic, lower Paleozoic, and Mesozoic sediments. Geological body Ar_3 is characterized by a relatively low gravity anomaly, high resistivity, and high magnetic susceptibility; it is thought to consist of Archean gneiss. Geological body M is characterized by a low gravity anomaly (−16 mGal), high magnetic susceptibility, and high resistivity (10^5 Ωm). Given that Mesozoic intrusive rocks are exposed in this location, geological body M is inferred to be Mesozoic granite. The crustal structure along NGP IV can be divided structurally into the Jiao–Liao–Ji Belt in the south and a Mesozoic granite intrusion zone in the north.

5.5 The deep geological structure, NGP V

NGP V (Figure 6), survey points 1–3 pass through the Benxi Basin, where the thickness of the Neoproterozoic–Mesozoic sedimentary cover reaches 5 km, overlying Neoarchean basement gneiss. The high gravity and magnetic anomalies in the vicinity of survey points 2–3 imply the presence of Archean supracrustal rocks beneath the sedimentary cover, making this area a good iron-ore prospect. The low gravity anomaly (−15 mGal) exhibited by geological body Ar_3 is attributed to Neoarchean basement gneiss, and its low resistivity is inferred to be due to the presence of fluid-filled fractures between survey points 3 and 4. Geological body M is characterized by a low gravity anomaly (−35 mGal) and high resistivity (10^6 Ωm), and the corresponding rock exposures comprise Mesozoic granite; thus, it is inferred that M is Mesozoic granite. To the north of geological body M, exposed rocks comprise mainly Archean gneiss, whereas to the south of geological body M, predominantly Paleoproterozoic strata are exposed. Therefore, it is inferred that M is located in the transition zone between the Jiao–Liao–Ji Belt and the Longgang Block. Geological body M inferred intruded along the basin-controlling fault of the Jiao–Liao–Ji Belt, which is located between survey points 6 and 7. Geological body T exhibits a gravity anomaly of −15 mGal, a resistivity of 10^3 Ωm, and a magnetic anomaly of 0 nT, body T is inferred to comprise a Late Triassic alkaline complex. The crustal structure along NGP V can therefore be divided into three structural units: the Longgang Block, a Mesozoic granite intrusion zone, and a Late Triassic alkaline complex.

6 Three-dimensional geological modeling

6.1 Cross-sections and gravity–magnetic joint inversion

In order to elucidate the deep geological structures in the study area in detail, on the basis of five nonseismic geological sections, eight vertical and four horizontal control grids were set up to divide the study area evenly. Based on 1:2,50,00,000-scale geological map data and 1:2,00,00,000-scale gravity and magnetic map data, we obtained gravity and magnetic curves and the boundary of geological bodies at the control grid by applying BIGMod software (Jilin University). Based on the surface boundary of the geological bodies, occurrence and regional geological data, the Speculative geological profile with the depth of 10 km was drawn at the control grid.

The detailed underground shapes of the geological bodies at the control grid were determined by GM-SYS Profile, an extension module of the software Geosoft Oasis montaj (https://www.geosoft.com/). GM-SYS calculates the gravity and magnetic model response and interactively manipulating models through forward modeling to fit observed gravity and magnetic data. First, the tool CVTGMS in GM-SYS was utilized to establish an inversion model based on the speculative geological profile, which mainly checks the closure of geological bodies on the profile and the correctness of topological relationship between geological bodies. Before running the model, it is necessary to set the geographic parameters such as profile coordinates and projection mode. The projection mode was set as 6-degree Gauss-kruger zone 21 in order to match with the geological map. In addition, parameters such as geomagnetic reference, longitude, latitude, and elevation of the study area are required for inversion of magnetic data to calculate the field strength, dip angle, and deflection angle of the study area and we set the geomagnetic reference to IGRF in this paper.

The Model Window consists of three panes from top to bottom: magnetics, gravity, cross section (Figure 7). Before the inversion, the measured gravity and magnetic curves at the control grid obtained by the cutting profile software was imported into the Gravity and Magnetic panes. In the Cross Section pane, the density, magnetic susceptibility, and residual magnetic susceptibility measurement value (Tables 1 and 2) of the geological body on the Speculative geological profile was defined. After setting the gravity and magnetic values of the geological body, the calculated gravity and magnetic anomaly curve of the profile can be displayed in the gravity and magnetic panes.

After the data are ready, the gravity and magnetic joint inversion by human–computer interaction is started. On the premise of keeping the topological relationship of geological bodies on the profile unchanged, the inversion method in the Cross Section pane was constrained by NGPs, geological body surface occurrences and borehole data, then the shape and depth of the geological body on the profile was manually adjusted. While adjusting the profile, the computer calculates the gravity and magnetic response in real time in the gravity and magnetic panes. Through repeated adjustment, the calculated gravity and magnetic anomaly curve (black thin line in Figure 7) is compared with the measured gravity and magnetic curve (black thick line in Figure 7). When the two are basically fitted, it can be considered that the adjusted profile better reflects the underground geological structure and physical characteristics of the stratum.

Figure 7 shows an example of one of the deep geological profiles, obtained from the fitting of control grid VI. At the southern end of the profile, the lower Paleozoic Liaohe Group is seen to be very thick. Owing to the high density of the Liaohe Group, the gravity anomaly in this area is high. The northern part of the Liaohe Group comprises Neoarchean gneiss that overlies Mesozoic rocks. The Neoarchean gneiss and Mesozoic rocks both exhibit low densities, resulting in a low gravity anomaly in this area. The northern part of the Neoarchean gneiss coincides with the Taizi River Depression. The depression has a synclinal structure comprising Archean supracrustal rocks overlain by the Paleoproterozoic Langzishan Formation and Neoproterozoic–Paleozoic sediments. The Archean supracrustal rocks become gradually shallower further to the north. Owing to the high density of the supracrustal rocks, the

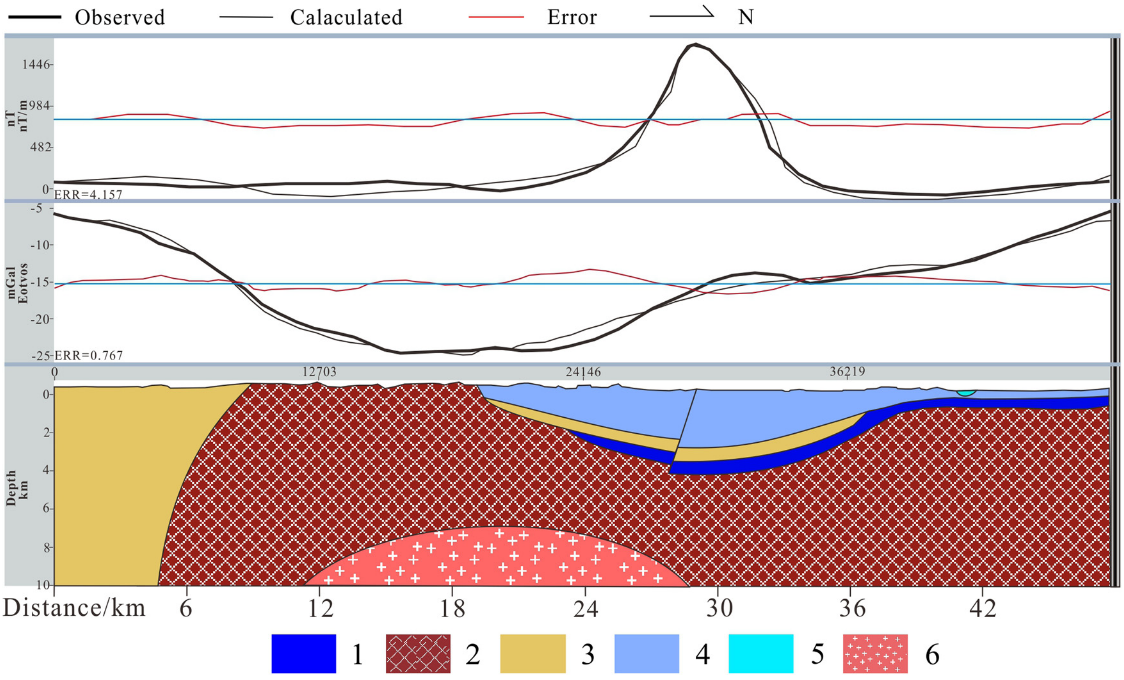

Figure 7: Deep geological profile by fitting of control section VI (see Figure 1 for location). (1) Archean supracrustal rocks. (2) Archean gneiss. (3) Paleoproterozoic unit. (4) Paleozoic unit. (5) Mesozoic unit. (6) Mesozoic granite.

gravity anomaly in the corresponding area is high. The same methodology and rationale were applied to the other 11 control grids to obtain the corresponding deep geological profiles.

6.2 Three-dimensional spatial modeling

The modeling method of this paper based on the section is one of the main 3D geological modeling methods at present [22–24]. The 3D spatial model is built by 3D visual modeling software of geological object computer aided design (GOCAD https://www.ring-team.org) developed by Nancy University of France. GOCAD has powerful 3D modeling, visualization, geological interpretation, and analysis capabilities.

During the data preparation period, 12 deep geological profiles completed by Geosoft software and the 5 NGPs were imported into GOCAD to generate a section inversion grid map of the study area (Figure 8) under identical coordinate systems, meanwhile, the surface boundary of the geological body with elevation information was inputted. Geological boundary data imported into GOCAD are classified and managed according to stratum boundary, rock boundary, fault boundary, etc. Afterwards the underground geological interface of geological body is generated by connecting the geological boundary in parallel section, cross section, and surface of the same geological body with the method of line-transfer-surface. The surface creation from Data and Borders with Bad Zs was employed to establish the surface interface of geological body combined with geological body surface boundary cutting DEM data. The generation of geological interface is the key to 3D modeling of GOCAD and is most workload. In order to ensure the closure of the geological body and the correctness of the topological relationship between the geological bodies, the boundary of the two intersecting geological interfaces should be the same geological boundary during the creation of the geological interface. Afterwards a closed surface model of geological body is created by using the method of surface modeling integrated with multiple geological interfaces of the same geological body. As a consequence, one or more geological bodies are displayed in three-dimension which can be treated as a basis to observe a single geological body's spatial distribution and spatial contact relationship between multiple geological bodies. Then the attribute model of geological body can be established by grid filling and assignment after establishment of the surface model [25]. In this paper, a three-dimensional deep geological surface model of Benxi iron-ore district is established as shown in Figure 9.

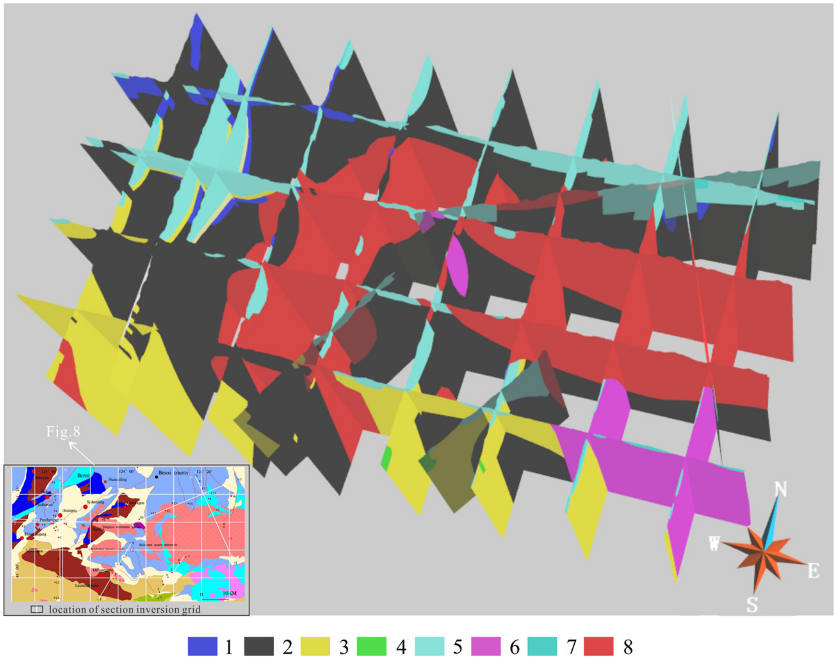

Figure 8: Section inversion grid chart of the Benxi area. (1) Archean supracrustal rocks. (2) Archean gneiss. (3) Paleoproterozoic unit. (4) Paleoproterozoic granite. (5) Neoproterozoic-Paleozoic unit. (6) Triassic complex rocks. (7) Mesozoic unit. (8) Mesozoic granite.

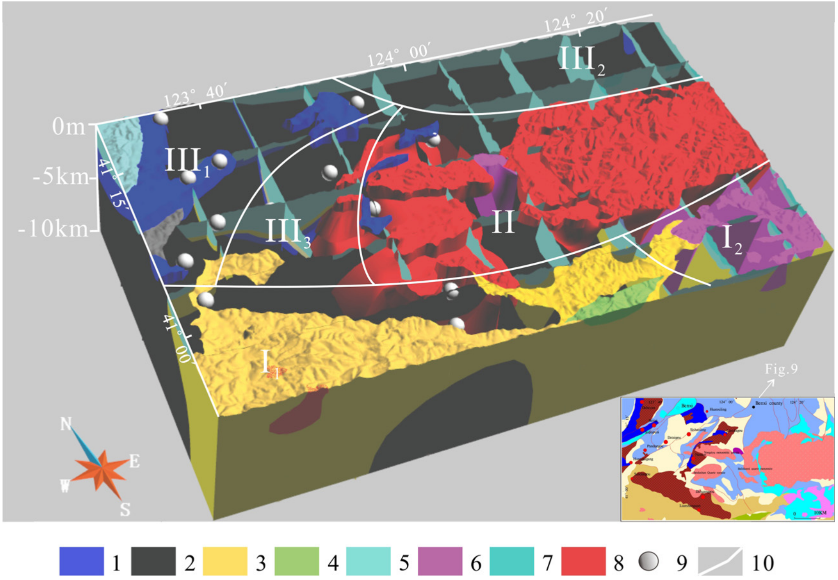

Figure 9: Deep three-dimensional geological model of the Benxi area. (1) Archean supracrustal rocks. (2) Archean gneiss. (3) Paleoproterozoic unit. (4) Paleoproterozoic granite. (5) Neoproterozoic-Paleozoic unit. (6) Triassic complex rocks. (7) Mesozoic unit. (8) Mesozoic granite. (9) BIF iron ore. (10) Demarcation line of tectonic unit.

7 Discussion

7.1 The deep geological structure of the Benxi area

According to the basement compositions, the spatial relationships between the basement and the cover, the compositions of the cover and the later transformations, the Benxi area can be divided into three first-order tectonic units (I–III): the Jiao–Liao–Ji Belt, a Mesozoic granite intrusion zone, and the Longgang Block, respectively. These can be further divided into six second-order tectonic units (Figure 9). The characteristics of each tectonic unit are described as follows.

Tectonic unit I_1 is located in the western part of the Jiao–Liao–Ji Belt. Owing to the high density of the Liaohe Group sediments, the gravity anomaly in this area is high, with the exception of two small low-gravity anomaly areas, which are caused by Paleoproterozoic and Mesozoic granite intrusions. Tectonic unit I_2 is located within the Saima–Aiyang Basin in the eastern part of the Jiao–Liao–Ji Belt. During the Triassic, this unit was intruded by the large-scale Saima alkaline complex, which is responsible for the low gravity and high magnetic property exhibited by the area. In the northern part of the Saima–Aiyang Basin, large-scale exhumed Cretaceous granite intrusions occur along the northern boundary of the Jiao–Liao–Ji Belt.

Tectonic unit II is located in the central part of the study area. The Mesozoic intrusives here are divided into eastern and western complexes. In the eastern part of the unit, an intrusion of Cretaceous age occurs along an E–W-oriented axis, large areas of which are exposed. The 3-D model shows that this intrusion is broad and shallow in the west but becomes narrower and deeper toward the east, reaching a depth of >10 km. In the western part of the unit, there are multiple intrusions that were emplaced along NE–SW-trending faults. There are many outcrops on the surface of the intrusions, and large concealed rock masses 1–2 km below the ground, the concealed rock masses extend westward to the vicinity of Dataigou.

Tectonic unit III_1 is located in the northwestern corner of the study area. Archean supracrustal rocks and Neoarchean gneiss are widely exposed in the unit. Tectonic unit III_2 is located in the Benxi–Tianshifu Basin. The cover sediments are mainly of Neoproterozoic–Paleozoic age, and the basement comprises Archean gneiss. In some areas, Archean supracrustal rocks occur between the basement gneiss and the sedimentary cover. Tectonic unit III_3 is located within the tectonic and sedimentary boundary zone of the Jiao–Liao–Ji Belt. The sedimentary cover in the western part of the unit has been folded into a syncline and subsequently buried to a depth of >5 km. The eastern part of the unit has been intruded by Mesozoic granites.

Table 3: Categories and sub-categories of deep geological structure in the Benxi area

Category	Sub-categories and characteristics	Diagram of type	Tectonic unit
Paleoproterozoic sediments	Abundant Paleoproterozoic deposits. Locally, Paleoproterozoic granites were exposed	Figure 10a$_1$	I$_1$
	Neoproterozoic–Paleozoic–Mesozoic sediments overlying Paleoproterozoic sediments. Locally, Late Triassic alkaline intrusions are exposed at the surface	Figure 10a$_2$	I$_2$
Mesozoic granite intrusions	Large Mesozoic granite intrusions	Figure 10b	II
Two-layer structure of Archean crystalline basement with overlying sedimentary cover	Exhumed Archean basement (comprising Archean supracrustal rocks and inclusions of Neoarchean gneiss)	Figure 10c$_1$	III$_1$
	Neoproterozoic–Paleozoic–Mesozoic sediments overlying Archean basement	Figure 10c$_2$	III$_2$
	The Paleoproterozoic Langzishan Formation and Paleozoic–Mesozoic cover sediments overlying Archean basement, with Mesozoic granite intrusions	Figure 10c$_3$	III$_3$

Summarize the characteristics of tectonic units, the deep geological structure type of the Benxi area can be divided into three main categories and six sub-categories. The characteristics of deep geological structure types and corresponding tectonic units are shown in Table 3, and the schematic diagram of deep geological structure types are shown in Figure 10.

7.2 The relationship between BIF development and sedimentary cover

The iron-ore deposits in the Benxi area are distributed in tectonic units II, III$_1$, III$_2$, and III$_3$. The deposits in tectonic units II and III$_1$ are mostly shallow, whereas those in tectonic unit III$_2$ occur within Archean rocks

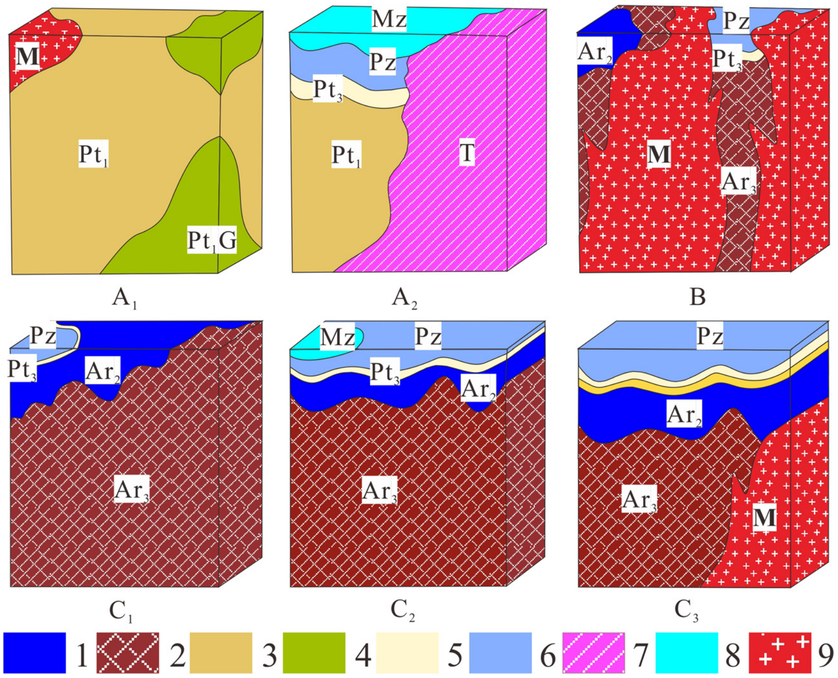

Figure 10: Diagram of deep geological structure types. (1) Archean supracrustal rocks. (2) Archean gneiss. (3) Paleoproterozoic unit. (4) Paleoproterozoic granite. (5) Neoproterozoic unit. (6) Paleozoic unit. (7) Late Triassic alkaline complex. (8) Mesozoic unit. (9) Mesozoic granite.

overlain by Neoproterozoic–Paleozoic cover sediments, and those in tectonic unit III_3 occur within Archean rocks overlain by the Paleoproterozoic Langzishan Formation and Neoproterozoic–Paleozoic cover sediments. The iron-ore deposits are concentrated mainly in tectonic unit III_3, which is likely due to the fact that tectonic unit III_3 is located within the sedimentary boundary of the Jiao–Liao–Ji Belt, where the Paleoproterozoic Langzishan Formation was deposited over Archean iron-bearing formations, entering the Paleoproterozoic. At the start of the Neoproterozoic, tectonic unit III_3 was located within the Taizi River Depression, and subsequently, a thick Neoproterozoic–Paleozoic cover sequence was deposited over the Langzishan Formation. As a result of the great thickness of the sedimentary cover, the iron-bearing formation in tectonic unit III_3 has been protected from weathering and denudation, enhancing its prospecting potential. In contrast, in the other tectonic units the iron-bearing formation has undergone significant weathering and denudation, due to extended periods of subaerial exposure, has been significantly degraded.

In short, due to the protection of sedimentary cover, the largest iron-ore deposits in Benxi area are mainly developed in tectonic unit III_3, on the contrary, the iron-ore deposits of other tectonic units are smaller in scale.

7.3 The influence of Mesozoic magmatic activity on BIF deposits

The model results (Figure 9) show that the Nanfen and Sishanling deposits are located above a large Mesozoic intrusion, which intruded into the lower parts of the deposit. In addition, the Nanfen deposit presents a low gravity anomaly (Figure 2 survey points 6–7), meaning that the Nanfen deposit does not exhibit the characteristics of high gravity anomaly that would be typically expected of iron-ore deposits, such as Dataigou deposit (Figure 3 survey points 4–5), this indicates that there exist erosion at the bottom of the Nanfen deposit, which caused the loss of iron. Therefore, the intrusion of Mesozoic rocks limiting iron-ore deposits prospecting potential.

Both the Nanfen and Sishanling deposits contain enriched iron ore. The Nanfen enriched iron ore occurs within interlayer voids along a fold axis within the host BIF. At the surface, the enriched ore crops out along strike for 100–150 m, with a thickness of 10–30 m, and typically extends for 700–800 m [26,27]. The Sishanling enriched iron ore only occurs locally, as the grade of the iron ore increases gradually with depth. Both the Benxi and Sishanling enriched iron ores have resulted from alteration processes, being derived from the local migration of iron during thermodynamic metamorphism of the host BIFs [26,28,29]. Thus, Mesozoic intrusive activity assisted the process of iron-ore enrichment in these areas. The intrusions would have released large volumes of hydrothermal fluid during crystallization, which would have traveled through fractures and faults within the host BIF, leaching the silica from the rock and subsequently enriching the iron.

7.4 Evolution of the deep geological structure of the Benxi area

During the early Archean (~3.8 Ga), the An-Ben land mass was formed [30–32]. Subsequently, between 2.8 and 2.6 Ga, the Archean supracrustal rocks of the Anshan Group, including large-scale BIFs, were deposited [33,34]. During the late Neoarchean (2.6–2.5 Ga), the region was subjected to large-scale intrusive magmatic activity [30,35–38], resulting in the formation of the intrusive rocks observed in NGPs II, III, and IV (Figures 3–5). The intrusion of magma caused the Archean supracrustal rocks to fragment and subsequently left them “floating” above Neoarchean gneiss. These rocks constitute the crystalline basement of the Longgang Block (Figure 11a).

During the early Paleoproterozoic, dextral shear movement of the TanLu Fault placed the An-Ben paleo-continent under a state of tension, resulting in extensional faulting and the formation of the Jiao–Liao–Ji Belt (Figure 11b; [39–42]). According to borehole data from the Dataigou and Sishanling iron-ore deposits, the Paleoproterozoic Langzishan Formation was deposited on top of the Archean iron-bearing formation. It is speculated that during the initial stages of formation of the Jiao–Liao–Ji Belt, the Langzishan Formation was laid down at Dataigou and Sishanling, as well as in areas to the south of these deposits. However, following the subsequent uplift of the Longgang Block, no later formations of the Liaohe Group were deposited within the Longgang Block. In contrast, the Jiao–Liao–Ji Belt underwent subsidence and thus received thick sedimentary sequences belonging to the Liaohe Group, consisting mainly of quartz sandstone, carbonaceous mudstone, and carbonate [16]. This thick Paleoproterozoic sedimentary rock sequence is observed in NGP II (Figure 3).

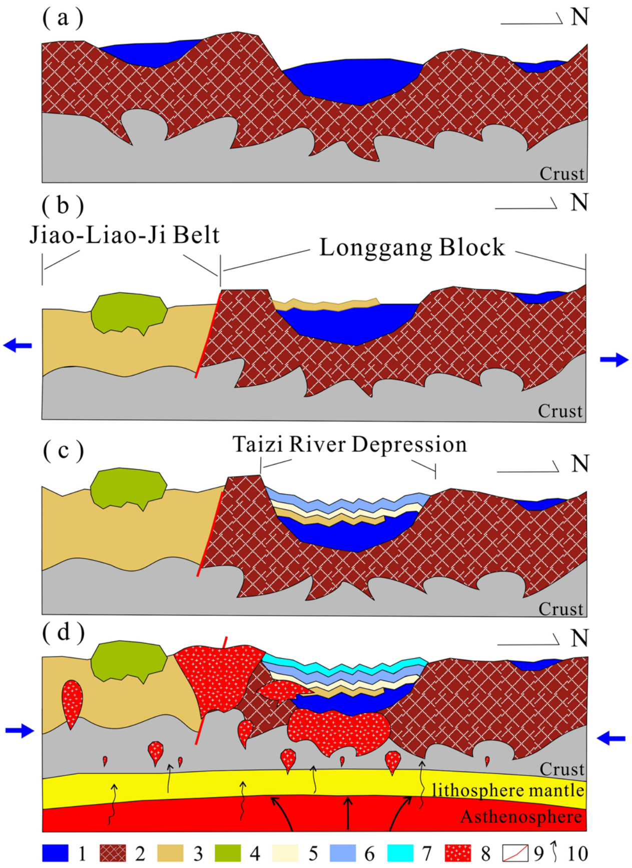

Figure 11: Deep geological structure evolution diagram of Benxi area. (a) Archean. (b) Paleoproterozaoic. (c) Neoproterozoic–Paleozoic. (d) Mesozoic. (1) Archean supracrustal rocks. (2) Archean gneiss. (3) Paleoproterozoic unit. (4) Paleoproterozoic granite. (5) Neoproterozoic unit. (6) Paleozoic unit. (7) Mesozoic unit. (8) Mesozoic granite. (9) Speculated normal fault. (10) Fluids.

From the Neoproterozoic, the Benxi area experienced relative tectonic quiescence and steady sedimentation. During the Neoproterozoic itself, the sandy–argillaceous Qingbaikou Formation was deposited at the site of the Liaodong aulacogen in the west of the study area. Sea-level rise during the Cambrian–Ordovician resulted in continued sedimentation within the Taizi River Depression, including the deposition of neritic–littoral facies strata. At the end of the Ordovician, the region once again underwent tectonic uplift, resulting in a sedimentary hiatus during the Silurian–Devonian. At the start of the Carboniferous, the study area was affected by oscillating marine transgressions and regressions, resulting in alternating marine and terrestrial facies of Carboniferous–Permian age [43]. The resultant sedimentary cover sequences of the Longgang Block are observed in NGPs II and V (Figures 3 and 6).

During the Mesozoic, the Paleo-Pacific plate was gradually subducted beneath the An-Ben continent [44–46]. Consequently, the sediments overlying the oceanic crust underwent dehydration, releasing water into the over-riding continental crust. This led to the partial melting of lower-crustal rocks in the over-riding plate and to the generation of granitic magmas (Figure 11d). The resulting granitic intrusions are observed in NGPs I, III, and V (Figures 2, 3, and 6).`

8 Conclusions

(1) A high-precision 3D model of the deep geological structure of the Benxi area was constructed through the acquisition and processing of NGPs. This model should prove extremely valuable in assisting iron-ore exploration in the area.

(2) The Benxi area can be divided into three first-order structural units on the basis of spatially variable structural characteristics: the Jiao–Liao–Ji Belt, a Mesozoic igneous intrusion zone, and the Longgang Block.

(3) There is a relationship between deep geological structure and iron-ore concentration in the Benxi area. Large and super-large ore deposits are concentrated within the tectonic and sedimentary boundary zone of the Jiao–Liao–Ji Belt. In areas where Archean supracrustal rocks are exposed, iron-ore deposits are of poorer quality, as the iron-bearing formations have been severely eroded.

(4) On the one hand, Mesozoic magmatic activity had a detrimental effect on the prospecting potential of the Benxi area, as the mechanical intrusion process caused erosion of the host BIFs. On the other hand, leaching of the host BIFs due to hydrothermal processes during magma intrusion has produced areas of concentrated high-grade iron ore.

Acknowledgments: This paper was based on the project of "Deep Geological Survey of Benxi-Linjiang area (Project No. 1212011220247)," supported by the National Geological Survey of China during the twelfth Five-year Plan "Three-dimensional Geological Mapping and Deep Geological Survey." Establishment of 3D virtual simulation model for medium and low temperature geothermal field (Project No. 20180520089JH), supported by Jilin Province Science and Technology Department Excellent Youth Talent Fund Project.

References

[1] Li SJ, Quan GX. Stratigraphic division and correlation of iron ore-bearing metamorphic rocks in Anshan-Benxi area. Contrib Geol Miner Resour Res. 2010;25(2):109–11 (in Chinese with English abstract).

[2] Song B, Zhao DM, Wan YS. Geochronology research of the iron formation of Gongehangling, Liaoning Province. Acta Petrol Mineral. 1992;11(4):317–23 (in Chinese with English abstract).

[3] Wang SL, Zang RH. U–Pb isotope age of individual zircon from biotite leptynite in the Qidashan iron deposit and its significance. Miner Depos. 1995;14(3):216–9 (in Chinese with English abstract).

[4] Dai YP, Zhang LC, Wang CL, Liu L, Cui ML, Zhu MT, et al. Genetic type, formation age and tectonic setting of the Waitoushan banded iron formation, Benxi, Liaoning Province. Acta Petrol Sin. 2012;28(11):3574–94 (in Chinese with English abstract).

[5] Zhang LC, Zhai MG, Wan YS, Quo J, Liu L. Study of the Precambrian BIF-iron deposits in the North China Craton: progresses and questions. Acta Petrol Sin. 2012;28(11):3431–45 (in Chinese with English abstract).

[6] Gross GA. A classification of iron formations based on depositional environments. Canadian Mineral. 1980;18(2):215–22.

[7] Zhou ST. The petrochemical study of the Archean banded iron deposit in Anshan-Benxi District, Liaoning Province. Bull Chinese Acad Geol Sci. 1987;2:139–53.

[8] Shen BF, Zhai AM, Yang CL, Cao XL. Temporal–spatial distribution and evolutional characters of Precambrian iron deposits in China. Geol Surv Res. 2005;28(4):196–206 (in Chinese with English abstract).

[9] Shen BF. Geological characters and resource prospect of the BIF type iron ore deposits in China. Acta Geol Sin. 2012;86(9):1376–95.

[10] Li H, Zhang Z, Li L, Zhang Z, Chen J, Yao T. Types and general characteristics of the BIF-related iron deposits in China. Ore Geol Rev. 2014;57(3):264–87.

[11] Zhai M, Windley BF, Sills JD. Archaean gneisses, amphibolites and banded iron-formations from the Anshan area of Liaoning Province, NE China: their geochemistry, metamorphism and petrogenesis. Precambrian Res. 1990;46(3):195–216.

[12] Xue LF, Dai CQ, Zhu M, Santosh M, Liu ZY. Anatomy of the Archean Anshan iron ore belt in the North China Craton: a geophysical approach. Precambrian Res. 2017;295:1–11.

[13] Hong XW, Pang HW, Liu XW, Li EF, Liu T. Geological characteristics of the Dataigou iron deposit in Benxi, Liaoning Province. Geol China. 2010;37(5):1426–33 (in Chinese with English abstract).

[14] Fan Z, Huang X, Tan L, Yang X, Zhang H, Zhou D, et al. A study of iron deposits in the Anshan area, China based on interactive inversion technique of gravity and magnetic anomalies. Ore Geol Rev. 2014;57(3):618–27.

[15] Peng C, Xue LF, Zhu M, Chai Y, Liu WY. The location and evolution of the tectonic boundary between the Paleoproterozoic Jiao–Liao–Ji Belt and the Longgang Block, northeast China. Precambrian Res. 2016;272:18–38.

[16] Liu FL, Liu PH, Wang F, Liu CH, Cai J. Progresses and overviews of voluminous meta-sedimentary series within the Paleoproterozoic Jiao–Liao–Ji orogenic/mobile belt, North China Craton. Acta Petrol Sin. 2015;31(10):2816–46 (in Chinese with English abstract).

[17] Hao DF, Li SZ, Zhao GC, Sun M, Han ZZ, Zhao GT. Origin and its constraint to tectonic evolution of Paleoproterozoic granitoids in the eastern Liaoning and Jilin province, North China. Acta Petrol Sin. 2004;20(6):1409–16 (in Chinese with English abstract).

[18] Lu XP, Wu FY, Lin JQ, Sun DY, Zhang YB, Guo CL. Geochronological successions of the early precambrian granitic magmatism in southern Liaodong peninsula and its constraints on tectonic evolution of the north china craton. Chinese J Geol. 2004;1:123–38 (in Chinese with English abstract).

[19] Fang RH, Wang BM, Shi JR, Zhuang ZB, Chen SB, Xiong LS, et al. Discovery History of Minerals in China (Volume of Liaoning). Beijing: Geological Publishing House; 1996. p. 16–43 (in Chinese with English abstract).

[20] Meng XY, Wang P, Zhang DY, Liang MJ. Element geochemistry of the Sishanling iron deposit in Liaoning Province and its geological implications. Geol China. 2012;39(6):1857–73 (in Chinese with English abstract).

[21] Zhang GR, Jiang SE, Yang ZX, Li CM, Guan PY, Han XP, et al. The features and forming mechanism of the Hanling-Pianling strike-slip fault zone in Liaoning Province, Northeast China. Earth Sci Front. 2004;3:183–92 (in Chinese with English abstract).

[22] Chen JP, Yu M, Yu PP, Shang BC, Zheng X, Wang LM. Method and practice of 3D geological modeling at key metallogenic belt with large and medium scale. Acta Geol Sin. 2014;88(6):1195–7.

[23] Xue LF, Li WQ, Zhang W, Chai SL, Liu ZH. A method of block-divided 3D geologic modeling in regional scale. J Jilin Univ (Earth Sci Ed). 2014;44(6):2051–8.

[24] Wang GC, Xu YX, Chen XJ, Guo JS, Yu JJ, Gong YM, Xiao L, Liu XG, Hua WH. Three-dimensional geological mapping and visualization of complex orogenic belts. Earth Sci J China Univ Geosci. 2015;40(3):397–406.

[25] Wu ZH, Guo FH, Li JT. The 3D modelling techniques of digital geological mapping. Arab J Geosci. 2019;12:467 doi: 10.1007/s12517-019-4615-6

[26] Wang SL. The genetic types of rich iron deposits of Anshan group in Anshan-Benxi area. Min Deposits. 1986;4:14–23 (in Chinese with English abstract).

[27] Zheng BD. Stratabound magnetite-rich deposits in Archean granitic greenstone terrane in Anshan-Benxi area, Liaoning Province. In: Wang KN, Yao PH, editors. A review of China's iron deposits. Beijing: Metallurgical Industry Press; 1992. p. 160–71.

[28] Cheng YQ. Problems on the genesis of the high-grade ore in the pre-sinian (pre-cambrian) banded iron ore deposits of the Anshan-type of Liaoning and Shandong provinces. Acta Geol Sin. 1957;37(2):153–80.

[29] Dai YP, Zhang LC, Zhu MT, Wang C, Liu L. Chentaigou BIF-type iron deposit, Anshan area associated with Archean crustal growth: constraints from zircon U-Pb dating and Hf isotope. Acta Petrol Sin. 2013;29(7):2537–50.

[30] Liu DY, Nutman AP, Compston W, Wu JS, Shen QH. Remnants of >3800 Ma crust in the Chinese part of the Sino-Korean Craton. Geology. 1992;20:339–42.

[31] Liu DY, Wan YS, Wu JS, Wilde SA, Zhou HY, Dong CY, et al. Chapter 3.5 Eoarchean Rocks and Zircons in the North China Craton. Dev Precambrian Geol. 2007;15(7):251–73.

[32] Liu DY, Wilde SA, Wan YS, Wu JS, Zhou HY, Dong CY. New U–Pb and Hf isotopic data confirm Anshan as the oldest preserved segment of the North China Craton. Am J Sci. 2008;308:200–31.

[33] Han C, Xiao W, Su B, Chen Z, Wang Z. Neoarchean Algoma-type banded iron formations from Eastern Hebei, North China Craton: SHRIMP U-Pb age, origin and tectonic setting. Precambrian Res. 2014;251(3):212–31.

[34] Wang C, Zhang L, Dai Y, Lia W. Source characteristics of the ~2.5 Ga Wangjiazhuang banded iron formation from the Wutai greenstone belt in the North China Craton: evidence from neodymium isotopes. Asian J Earth Sci. 2014;93:288–300.

[35] Jahn BM, Auvray B, Cornichet J, Bai YL, Liu DY. 3.5 Ga old amphibolites from eastern Hebei Province, China: field occurrence, petrography, Sm–Nd isochron age and REE geochemistry. Precambrian Res. 1987;34(3–4):311–46.

[36] Song B, Allen PN, Liu DY, Wu JS. 3800 to 2500 Ma crustal evolution in Anshan area of Liaoning Province, Northeastern China. Precambrian Res. 1996;78:79–94.

[37] Li SZ, Yang ZS. Types and genesis of Paleoproterozoic granites in the Jiao-Liao Massif. Northwest Geol. 1997;43:21–7 (in Chinese with English abstract).

[38] Zhu M, Dai Y, Zhang L, Wang C, Liu L. Geochronology and geochemistry of the Nanfen iron deposit in the Anshan-Benxi area, North China Craton: Implications for ~2.55 Ga crustal growth and the genesis of high-grade iron ores. Precambrian Res. 2015;260:23–38.

[39] Zhao GC, Wilde SA, Cawood PA, Sun M. Archean blocks and their boundaries in the North China Craton: lithological, geochemical, structural and P–T path constraints and tectonic evolution. Precambrian Res. 2001;107:45–73.

[40] Zhao GC, Sun M, Wilde SA, Li SZ. Late Archean to Paleoproterozoic evolution of the North China Craton: key issues revisited. Precambrian Res. 2005;136:177–202.

[41] Zhao GC. Metamorphic evolution of major tectonic units in the basement of the North China Craton: key issues and discussion. Acta Petrol Sin. 2009;5:1772–92.

[42] Li SZ, Zhao GC, Sun M, Han ZZ, Hao DF, Luo Y, Xia XP. Deformation history of the Paleoproterozoic Liaohe group in the eastern block of the North China Craton. Asian Earth Sci. 2005;24:659–74.

[43] Guo SZ, Zhang LD, Zhang CJ, Bao QZ, Peng YD. Proterozoic-Paleozoic Sequence Stratigraphy In The Taizi River Basin of Liaoning Province. J Precious Metall Geol. 2001;10(1):1–10 (in Chinese with English abstract).

[44] Zhou XM, Li WX. Origin of Late Mesozoic igneous rocks in Southeastern China: Implications for lithosphere subduction and underplating of mafic magmas. Tectonophysics. 2000;326(3–4):269–87.

[45] Chen B, Tian W, Zhai MG, Arakawa Y. Zircon U–Pb geochronology and geochemistry of Mesozoic magmatism in the Taihang Mountains and other places of the North Nhina Nraton, with implications for petrogenesis and geodynamic setting. Acta Petrol Sin. 2005;21(1):13–24 (in Chinese with English abstract).

[46] Wu FY, Yang JH, Wilde SA, Zhang XO. Geochronology, petrogenesis and tectonic implications of Jurassic granites in the Liaodong Peninsula, NE China. Chem Geol. 2005;221(1):127–56.